Available online at www.sciencedirect.com

ScienceDirect

Ceramics International 39 (2013) 8751–8759

CERAMICS INTERNATIONAL

www.elsevier.com/locate/ceramint

Effect of porosity on the microhardness testing of brittle ceramics: A case study on the system of NiO–ZrO_2

Qi Tang, Jianghong Gong*

State Key Laboratory of New Ceramics and Fine Processing, School of Materials Science and Engineering, Tsinghua University, Beijing 100084, PR China

Received 27 March 2013; received in revised form 17 April 2013; accepted 17 April 2013
Available online 23 April 2013

Abstract

Microhardness tests were conducted on a series of NiO–ZrO_2 ceramics with different porosities ranging from 2% to 18%. For each sample, the measured hardness decreases with increasing indentation load, showing a significant indentation size effect. The indentation data were analyzed according to the modified proportional specimen resistance (PSR) model and it was found that the resultant load-independent hardness decreases with increasing porosity. The porosity-dependence of the load-independent hardness was analyzed and a concept of true hardness was proposed to characterize the actual material resistance to indentation-induced plastic deformation. Furthermore, the applicability of the modified PSR model in describing the indentation size effect observed on porous materials is discussed.

Keywords: B. Porosity; C. Hardness; D. ZrO_2; Indentation size effect

1. Introduction

Microhardness is an important parameter often used to characterize the mechanical properties of a material on a microscopic scale. However, the variation of the measured hardness (the *apparent hardness*), traditionally defined as the ratio of the applied load, P, to the resultant indentation area, A, with the applied test load is widely reported [1–10]. The load dependence of the apparent hardness, sometimes referred to as *indentation size effect* (ISE), has been studied for several decades and several empirical or semi-empirical equations have been proposed to describe the ISE and yield the load-independent hardness number [11–16]. Most of these empirical or semi-empirical equations may be regarded to be a censored form of the polynomial series representation originally proposed by Bückle [17],

$$P = a_0 + a_1 d + a_2 d^2 + \cdots + a_n d^n \tag{1}$$

where P and d are the indentation load and the resultant indentation size, respectively, and a_i ($i=0, 1, 2,\ldots, n$) are adjustable parameters. It was usually suggested [11,12] that the a_0-term in Eq. (1) corresponds to a load threshold for an indenter to produce a permanent indentation and has such a small magnitude that it can be neglected in most situations. Moreover, a good fit of experimental data can be obtained utilizing only two of these power series, i.e. [2,11,12,18],

$$P = a_1 d + a_2 d^2 \tag{2}$$

The physical meanings of Eq. (2) have been explained in the proportional specimen resistance (PSR) model [12] and based on the energy-balance consideration [11], respectively. Both models, which were frequently employed to explore the origin of the experimentally observed ISE, suggest that the coefficient a_2 can be considered to be a measure of the load-independent hardness, H_0, of the test material,

$$H_0 = k a_2 \tag{3}$$

where k is a constant dependent of the indenter geometry. For the conventionally used Vickers indenter, $k=1.8544$.

A series of works conducted by Gong et al. [13,14,19–22] showed that, when analyzing the indentation data measured on brittle ceramics according to Eq. (1), the a_0-term is larger and cannot be neglected in some cases. Therefore, the relationship between the indentation load and the resultant indentation size

*Corresponding author. Tel.: +86 10 62772855; fax: +86 10 62771160.
E-mail address: gong@tsinghua.edu.cn (J. Gong).

0272-8842/$ - see front matter © 2013 Elsevier Ltd and Techna Group S.r.l. All rights reserved.
http://dx.doi.org/10.1016/j.ceramint.2013.04.061

should be described properly with [13,14]

$$P = a_0 + a_1 d + a_2 d^2 \quad (4)$$

The physical meanings of the a_0-term were discussed in detail based on the analyses of the effects of the machining-induced plastically deformed surface [13] and the experimental errors related to the smallness of the indentation on the hardness measurements [14]. Similarly, the a_2-term was also suggested to be related to the load-independent hardness with Eq. (3).

The applicability of Eq. (4), frequently referred to as the modified PSR model, in describing the ISE has been examined by many authors on different materials [7,9,23–28]. In most situations, it was suggested that the experimental data may be described satisfactorily with Eq. (4) and the resultant load-independent hardness, H_0, may be related reasonably to the chemical composition, grain size and processing procedures, etc. However, some exceptions were also reported. For example, Kim and Kim [6] found that a negative value of a_2 was obtained when analyzing the indentation data measured on some traditional ceramics (roofing tiles) with Eq. (4). This experimental result implies that, for the materials with higher porosities, it seems to be unreliable to use the parameter a_2 as an index of the load-independent hardness.

There have been several papers concerning the effect of porosity on the measurement of the apparent hardness and it was generally reported that the apparent hardness decreases with the increasing porosity, or the decreasing relative density [1,3,4,29,30]. A little effort has also been devoted to the effect of porosity on the determination of load-independent hardness from the existing models. Gong [31] conducted a simple and phenomenological analysis based on the energy-balance consideration and pointed out that the parameter a_2 includes not only the energy needed for producing the permanent plastic deformation but also the effect of the changes in free surface energy due to the densification of the pores in the prospective indentation deformation zone. Furthermore, Tricoteaux et al. [32] analyzed the ISE observed on a series of β-tricalcium phosphate (β–TCP) ceramics based on the strain gradient plasticity theory to yield the macrohardness number, which is similar to the load-independent hardness mentioned here. They found that the macrohardness decreases with increasing porosity and, according to their results, a negative macrohardness number may also be predicted when the porosity is larger enough, say about 30%.

Note that Gong's work [31] only presents a simple analysis for the effect of porosity on the load-independent hardness without any experimental verification. As a complement to Gong's work, indentation tests were conducted in this study on a series of NiO–ZrO_2 samples with different porosities and the observed indentation size effects were analyzed according to Eq. (4). It will be shown that Gong's work provides a satisfactory description for the porosity dependence of the load-independent hardness. Furthermore, the difference between the two concepts, the *load-independent hardness* and the *true hardness*, are discussed in detail based on the analysis of the effect of porosity on the hardness measurements.

Table 1
Chemical compositions and densities of experimental samples.

Sample	Composition (wt%)		Density ρ (g/cm^3)	Total porosity p (%)
	NiO/8YSZ	PMMA		
NY00	100	0	6.271	2.19
NY05	95	5	6.216	3.05
NY10	90	10	5.963	6.98
NY15	85	15	5.538	13.62
NY20	80	20	5.240	18.27

2. Experimental

2.1. Preparation and characterization of the test material

The materials examined in the present study are a series of composites composed of 58 wt% NiO and 42 wt% cubic ZrO_2 (stabilized with 8 mol% Y_2O_3, YSZ).

To prepare these composites, the mixed NiO/ZrO_2/Y_2O_3 powder was synthesized firstly via a co-precipitation method using a mixed solution of 0.5 M $NH_3 \cdot H_2O$ and 0.5 M NH_4HCO_3 with a certain proportion as the precipitant. The mixture with an appropriate proportion of 1 mol/L $Ni(NO_3)_2$, 1 mol/L $ZrOCl_2$ and 0.5 mol/L $Y(NO_3)_3$ solutions was dripped gradually into the appropriately excessive $NH_3 \cdot H_2O$–NH_4HCO_3 solution to form precipitate. The precipitate was washed, filtered, fried and calcined at 800 °C for 2 h to form the mixed NiO/ZrO_2/Y_2O_3 powder. Then the mixed NiO/ZrO_2/Y_2O_3 powder was mixed with different contents of PMMA (see Table 1) and cold isostatic-pressed into disks under 200 MPa. Finally, the disks were sintered to form the required composites ceramics. During the sintering of the disks, a slow heating rate of 1 °C/min was set for the temperature ranging from room temperature to 425 °C to ensure the completely wipe-off of the PMMA and then the temperature was increased to 1400 °C at a heating rate of 5 °C and held at 1400 °C for 2 h.

The phase constitutions of the sintered samples were analyzed by X-ray diffraction (XRD) and the data indicate that only two phases, NiO and cubic ZrO_2, exist in the sintered samples. The densities were measured using Achimedes' method. Using the theoretical density of $\rho_{th} = 6.411$ g/cm^3, which was determined based on the measured lattice parameter and rule of mixture, the porosity of each sample was calculated from the measured density and the results are also listed in Table 1.

The microstructures were examined by scanning electron microscope (SEM). Fig. 1 shows the typical microstructures of the surfaces of the samples NY00, NY10 and NY20. As can be seen, the porosity and the size of the pores increase with increasing amount of PMMA.

2.2. Hardness testing

Vickers indentation tests were conducted on the polished surface of each sample in the load range from 0.49 to 4.9 N using a commercial low-load hardness tester. All the

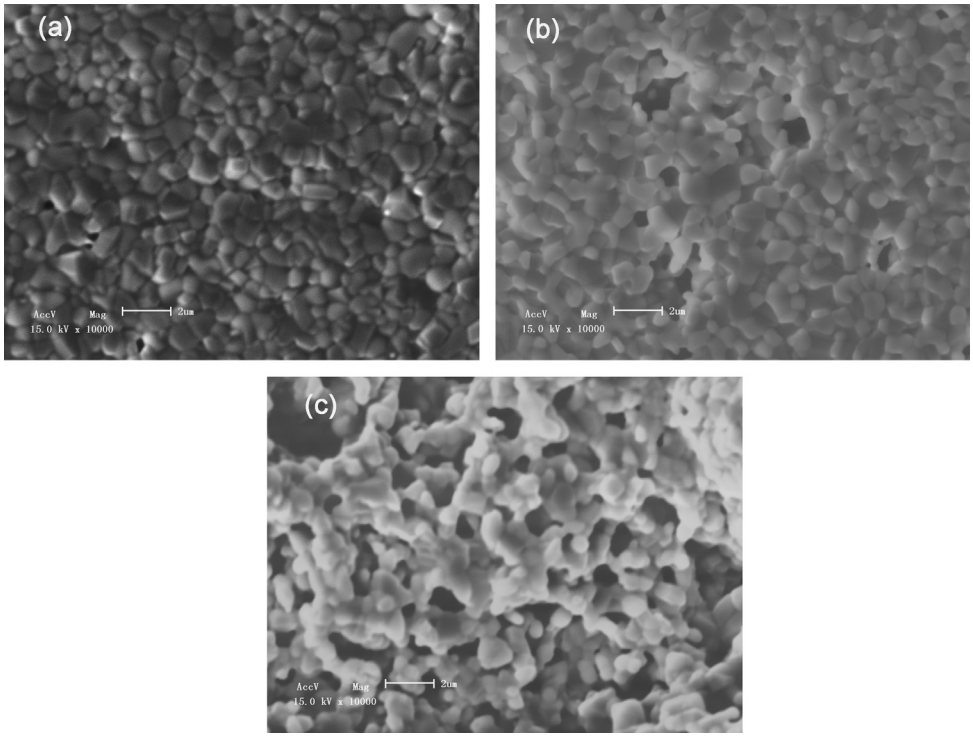

Fig. 1. SEM images of the surface of samples (a) NY00, (b) NY10 and (c) NY20.

indentation tests were performed under ambient laboratory conditions with a constant indenter dwell time of 15 s. After the indentation cycle has been completed, the lengths of the two diagonals of each indentation impression were measured using an optical microscopy with a magnification of 400 and an error of measurement of ± 0.02 μm. It should be pointed out that the existence of a large amount of pores in the sample surfaces would result in the occasional formation of irregular indentation impressions. In the present study, only the well-formed square-shaped indentation impressions are considered to be effective and used for the following analyses. At each applied load, 100 effective indentation impressions were made and measured for each sample except the sample NY00 for which only 30 impressions were made because of the small variation in the resultant indentation sizes.

3. Results

The apparent hardness, H, was calculated using the experimental measured indentation size, d, and the corresponding applied load, P, with $H = 1.8544P/d^2$, for the five samples and the results are shown in Fig. 2. Three interesting features of Fig. 2 should be noted: (1) At a given applied load level, the apparent hardness decreases with increasing porosity, being in consistence with the results reported by other authors [1,3,4,29,30]. (2) The standard deviation of the apparent hardness increases with the porosity. This can be understood easily by considering the statistical distribution of the pores in the surface of the test samples, see Fig. 1. (3) Evidently, the apparent hardness decreases with increasing applied load for each sample, exhibiting significant indentation size effect.

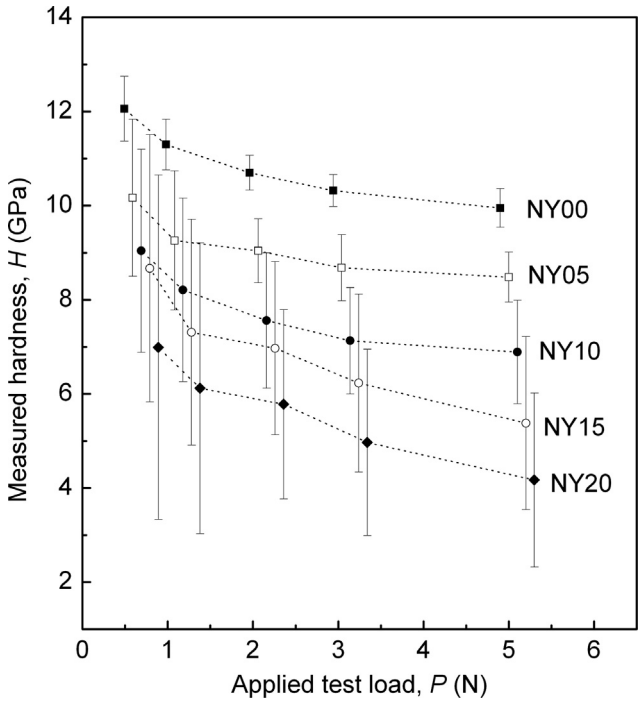

Fig. 2. Apparent hardness and function of the applied test load for all test samples. Points and error bars represent mean ± standard deviation. The points have been slightly shifted for clarity.

The applications of Eq. (4), the modified PSR model, to all the test samples are now illustration in Fig. 3, where the applied test load is plotted as functions of the resultant indentation size. For the sake of conciseness, all the error bars corresponding to each data point are omitted in this figure.

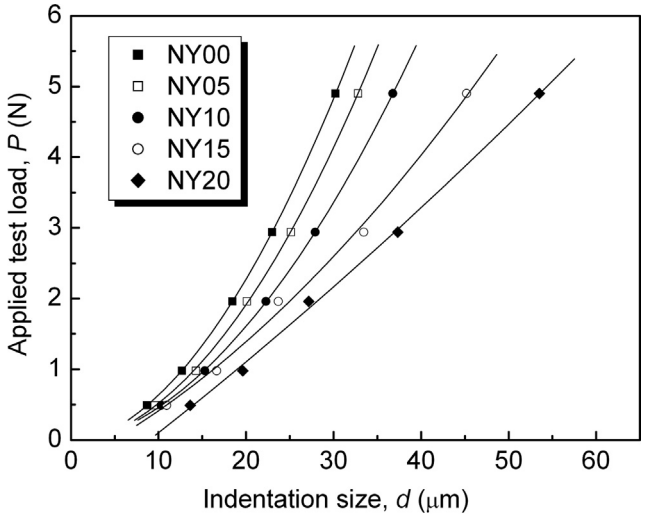

Fig. 3. Indentation size versus the applied test load for the test samples.

The solid lines in these plots are obtained by a conventional polynomial regression analysis according to Eq. (4). Clearly, Eq. (4) is proven sufficiently suitable for the representation of the experimental data for all the samples, although the porosity of the sample varies from about 2% to about 20%. The best-fit values of the parameters included in Eq. (4) are summarized in Table 2. It is clearly that the best-fit value of a_2, which directly relates to the load-independent hardness Eq. (3), decreases with increasing porosity although all the five samples have the same compositions and were fabricated according to the nearly same procedures.

It is of interest to analyze the experimental data according to Eq. (3), the PSR model. Rewriting Eq. (3) as

$$\frac{P}{d} = a_1 + a_2 d \tag{5}$$

Eq. (5) predicts a linear relationship between P/d and d. Some of the experimental data obtained in the present study are now re-plotted in Fig. 4 in a P/d–d scale. As can be seen, within the examined range of the applied test load, a good linear relationship was observed for the sample with the smallest porosity. For the sample with the largest porosity, NY20, however, the experimental data evidently fall into two separate sets, further verifying the conclusion yielded in many of the previous studies that the PSR model is no sufficient for the description of the ISE observed in ceramics. Thus, it can be concluded that, for the porous materials, the modified PSR is also more suitable than the PSR model for the description of the indentation data.

4. Discussion

4.1. Theoretical consideration

In order to give a possible explanation for the experimental fact that the load-independent hardness deduced based on Eq. (4) decreases with increasing porosity, here we recall the analysis conducted by Gong [31].

Table 2
Regression analysis results of the experimental data according to Eq. (4).

Sample	a_0 (N)	a_1 (N/mm)	a_2 (N/mm^2)	Correlation factor
NY00	−0.081	25.44	4608.6	1.0000
NY05	−0.052	15.66	4128.4	0.9998
NY10	−0.071	22.57	3060.3	0.9999
NY15	−0.332	63.11	1148.3	0.9965
NY20	−0.842	91.58	291.6	0.9983

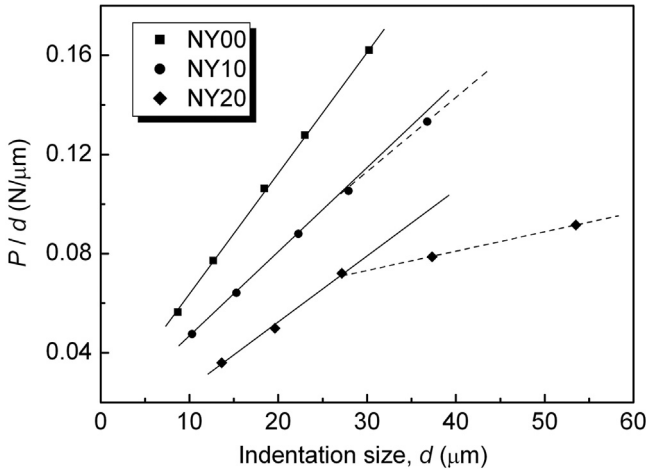

Fig. 4. P/d plotted against d for samples NY00, NY10 and NY20.

Enlightened by the work of Kim and Kim [6] on porous traditional ceramics, Gong conducted a simple and phenomenological analysis for the effect of porosity on the load-independent hardness [31]. Gong's analysis starts from an energy-balance consideration for the indentation procedure. To a first approximation, during an indentation event, the work done by the applied test applied, proportional to Pd, is transformed into a strain energy component, proportional to the volume of the resultant indentation impression ($\propto d^3$), and a surface energy component, proportional to the area of the resultant impression ($\propto d^2$) [11,14]. This results in a general form to relate the indentation size with the applied test load,

$$Pd = a_1 d^2 + a_2 d^3 \tag{6}$$

Dividing both sides of Eq. (6) by d would yield Eq. (2).

It is generally assumed that the permanent plastic deformation is the only source of the volume change during indentation. Consequently, the parameter a_2 included in Eq. (6), having a dimension of J/m^3 (N/m^2), is considered as a measure of the energy, γ, needed for producing the permanent plastic deformation of an unit volume and, thus, to be related directly to hardness, an index of material resistance to indentation-induced plastic deformation [11,14]. This seems to be true when the test material has a very small porosity. However, the effect of the densification of pores during indentation should be incorporated into Eq. (6) if the porosity of the test material is large enough.

Considering a materials with a porosity of p. For the sake of simplification, the pores in the material were assumed to be spherical in shape with the same radius of r. During indentation, the pores in the prospective indentation zone would be compressed, resulting in a change in free surface area, ΔS_p. Assuming the deformed pore to a circle in shape, we can obtain

$$\Delta S_p = N(4\pi r^2 - \pi r^2) = 3N\pi r^2 \tag{7}$$

where N is the number of the pores in the prospective indentation zone and can be determined from

$$p = \frac{V_p}{V_0} = \frac{N(4\pi r^3/3)}{d^2} h/6 \propto 2N\left(\frac{r}{d}\right)^3 \tag{8}$$

where V_p is the total volume of the pores in the prospective indentation zone before indentation, and V_0 and h are the volume and the depth of the indentation impression ($h \propto d$).

Note that the porosity can also be expressed as $p = N_0(4\pi r^3/3) \propto r^3$ (where N_0 is the number of pores in the unit volume), Combining Eqs. (7) and (8) yields

$$\Delta S_p \propto p^{2/3} d^3 \tag{9}$$

Incorporating the energy change due to the pore densification into the energy balance equation, Eq. (6) (here we let $a_2 = \gamma$ to describe the energy concerning only the plastic deformation), we obtain

$$Pd = (a_1 d^2 - \beta' \Delta S_p) + \gamma\, d^3 \tag{10}$$

where β' is a constants. The minus in the parentheses is introduced because the changes in the shapes of the pores would result in a decrease in the area of the free surface. Inserting Eq. (9) into Eq. (10) gives

$$P = a_1 d + (-\beta\, p^{2/3} + \gamma) d^2 \tag{11}$$

where β is another constant.

It should be pointed out that the above analysis is based on the original energy-balance consideration proposed by Fröhlich et al. [11]. If the systematical experimental errors in the measured indentation size and the measured test load, resulting from the optical resolution of the objective lens and/or the sensitivity of the load cell, are considered further, a constant term, a_0, should be introduced and Eq. (11) should be further modified to a form similar to Eq. (4) [14].

Comparing Eq. (11) with Eq. (4) gives

$$a_2 = -\beta\, p^{2/3} + \gamma \tag{12}$$

Eq. (12) is the basic equation deduced in Gong's work [31] to consider the effect of porosity on the determination of the load-independent hardness with Eqs. (4) and (3). As predicted by Eqs. (12), a_2 would decrease with increasing porosity and change from positive to negative when the porosity is large enough. With this equation, it is easy to explain why the best-fit value of a_2 is negative for the traditional ceramics examined by Kim and Kim [6].

4.2. Experimental verification

The experimental results obtained in the present study (Table 2) provide a solid support for the validity of Eq. (12). Fig. 5 shows the best-fit value of a_2 as a function of the porosity for the NiO–ZrO_2 samples. In the a_2 versus $p^{2/3}$ scale, a linear relationship exists, being in agreement with the prediction of Eq. (12).

Similar conclusion can also be deduced by analyzing the experimental results reported by Tricoteaux et al. [32] on a series of porous β-TCP ceramics with different porosities. Tricoteaux et al. did not report the original indentation data in their work but they indicated that the experimental data could be described satisfactory with the strain gradient plasticity theory proposed by Nix and Gao [33],

$$H^2 = H_{M0}^2 + \frac{H_{LSF}^2}{h} \tag{13}$$

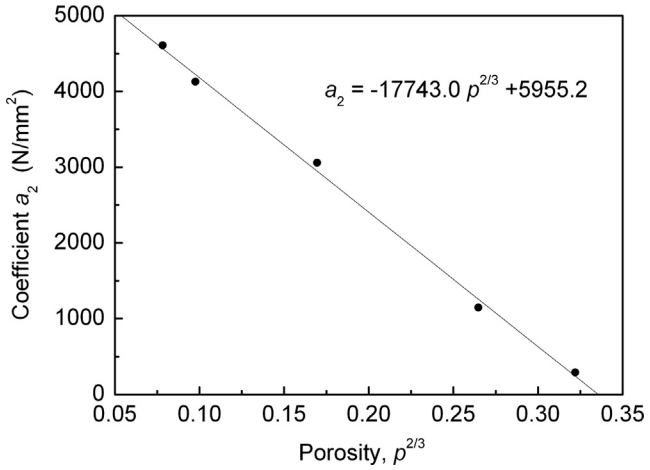

Fig. 5. Variation of the best-fit value of the parameter a_2 with the porosity, p, for the NiO–ZrO_2 samples.

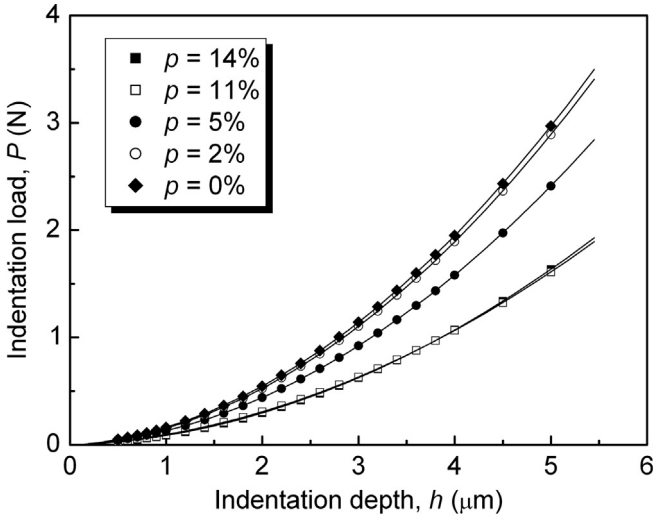

Fig. 6. Indentation depth versus the applied test load for porous β-TCP ceramics. Data points correspond to the results calculated, rather than measured, using the regression analysis results reported in Ref. [32].

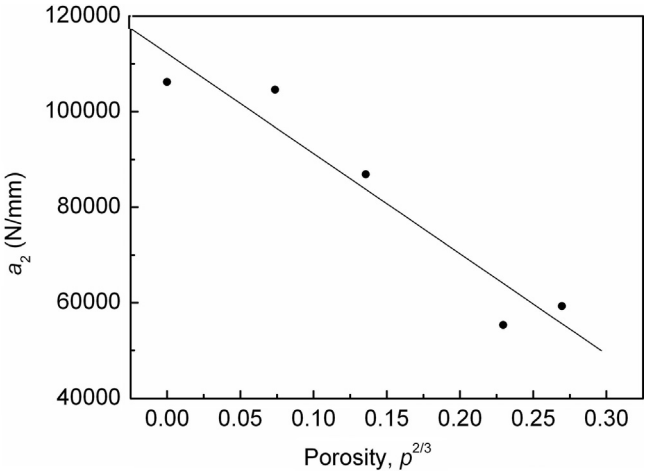

Fig. 7. Variation of the best-fit value of the parameter a_2 with the porosity, p, for porous β-TCP ceramics.

where h is the indentation depth and H_{M0} and H_{LSF} are constants. Using the best-fit values of H_{M0} and H_{LSF} listed in Table 4 of Ref. [32], the applied test load P can be calculated as a function of the indentation depth, h, based on Eq. (7) within the examined range of indentation depth (about 0.5–5 μm), and the results are now shown in Fig. 6 (points). Also shown in Fig. 6 are the best-fit lines of the "experimental" data according to Eq. (4). Again, the experimental results verify the applicability of Eq. (4). The best-fit value of a_2 is plotted as a function of the porosity in Fig. 7. Although there is a somewhat lager scatter in the data, a linear relationship between a_2 and $p^{2/3}$ is evident.

4.3. Further comments

Having concluded that the porosity of the test materials would play an important role on the determination of the load-independent hardness based the energy-balance consideration or the (modified) PSR model, some further comments should be made.

The first comment concerns the physical meanings of the load-independent hardness calculated from a_2 with Eq. (2). As indicated by Eqs. (12), a_2 includes both the energy changes due to the densification of the pores ($\propto \beta p^{2/3}$) and plastic deformation ($\propto \gamma$). Therefore, the load-independent hardness calculated with Eq. (2), i.e., $H_0 = ka_2$, represents the materials resistance to the *total* volume deformation and cannot be treated as a measure of the material resistance to indentation-induced plastic deformation. The actual material resistance to indentation-induced plastic deformation should be expressed by

$$H_T = k\gamma \tag{14}$$

To distinguish between H_0 and H_T, we call H_T as the *true hardness* of the test material.

In the previous studies [11–16,19–28] concerning the determination of the load-independent hardness based on Eq. (4) or Eq. (2), the two concepts, the *load-independent hardness* and the *true hardness*, were usually considered to be the same. This is not a problem if the test materials are dense with porosities typically smaller than 1%. In these situations, the effect of porosity may be ignored and the resultant a_2 is nearly equal to γ, giving a reasonable approximation of the true hardness for the test material. If the test material has a large porosity, however, the load-independent hardness, H_0, would be influenced significantly by the porosity according to Eq. (12) and exhibit a value smaller than the true hardness, H_T. As an example, the load-independent hardness of the materials examined in the present study varies from 8.6 GPa ($a_2 = 4608.6$ N/mm^2) to 0.5 GPa ($a_2 = 291.6$ N/mm^2) when the porosity increases from 2% to 18%, while the true hardness of the samples should be a porosity-independent parameter and may be roughly estimated to be about 11.0 GPa ($\gamma = 5955.2$ N/mm^2, Fig. 5).

Another comment concerns the applicability of Eq. (4) in describing the indentation data for porous materials. Although the experimental results shown in Figs. 3 and 6 prove that Eq. (4) may be used to describe the indentation data measured on materials with high porosities, it should be noted that the correlation factor of the polynomial regression exhibit a decreasing tendency as the porosity increases (Table 2). In fact, an interesting feature can be found when we examine the experimental data much carefully. The experimental data for the samples NY00 and NY20 are now re-plotted in Fig. 8. The solid lines in this plot were obtained by polynomial regression of the first three data points (the solid symbols in the figure) according to Eq. (4). For the sample NY00 which has the smallest porosity, the data points measured at higher load levels (open symbols) fall along the solid line, indicating that the indentation data can be described satisfactory with Eq. (4) within the whole examined range of indentation load. For the sample NY20 with the largest porosity, however, the data points measured at higher load levels (open symbols) deviate evidently from the solid line.

Similar phenomenon was also observed when analyzing the experimental data reported by Kim and Kim on porous

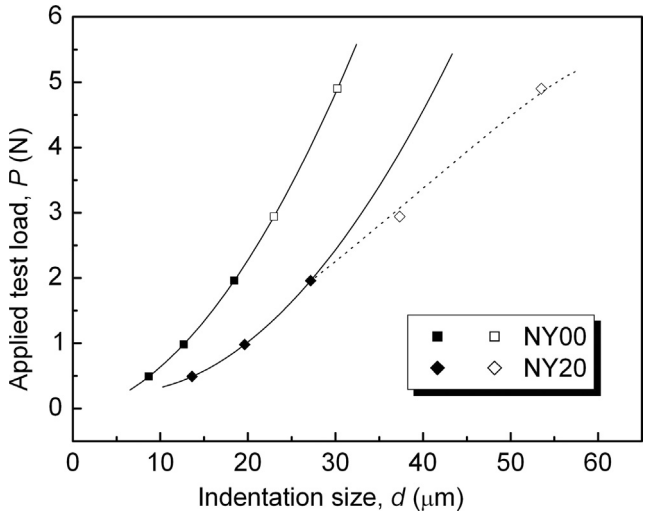

Fig. 8. Re-examination of the indentation data for the samples NY00 and NY20 to show the deviations from the prediction of Eq. (4).

traditional ceramics. Fig. 9 is plotted using the experimental data listed in Table 2 of Ref. [6] for the sample MS. The tendency shown in this figure is similar to that for sample NY20 in Fig. 8.

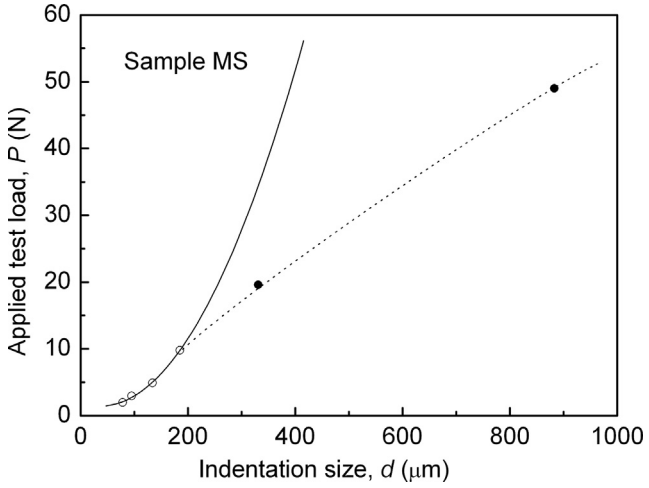

Fig. 9. Indentation size versus the applied test load for a roofing tile with a porosity of 44.4%. Data from Ref. [6].

From the viewpoint of energy-balance, the deviation of the experimental data measured at higher load levels from the prediction of Equation clearly implies that, for highly porous materials, there exist some new mechanisms which may result in energy changes, thereby making the expression of a_2 more complicated than Eq. (12). At least, collapses would be expected for materials with large porosity when being indented at higher loads. In addition, extensive microcracking would also occur at high load levels for brittle materials. Fig. 10 compares the typical indentation impressions made at different loads for the samples NY00 and NY20. For the dense material (NY00), the impressions always keep a regular square shape without any clear-cut microcracks or collapses. The indentation impression made at low loads on porous material (NY20) is similar to that observed for dense material. At higher loads, however, evident collapses and lateral cracking occur. These features may be the main sources that result in the derivation of the experimental data from the prediction of Eq. (4).

The analysis conducted above may be extended further into a general consideration. Undoubtedly, there exist in materials many mechanisms which may result in energy changes during an indentation event and different mechanisms would be initiated at different load levels. Thus, the exact form of the expression for the parameter a_2 should be different in different

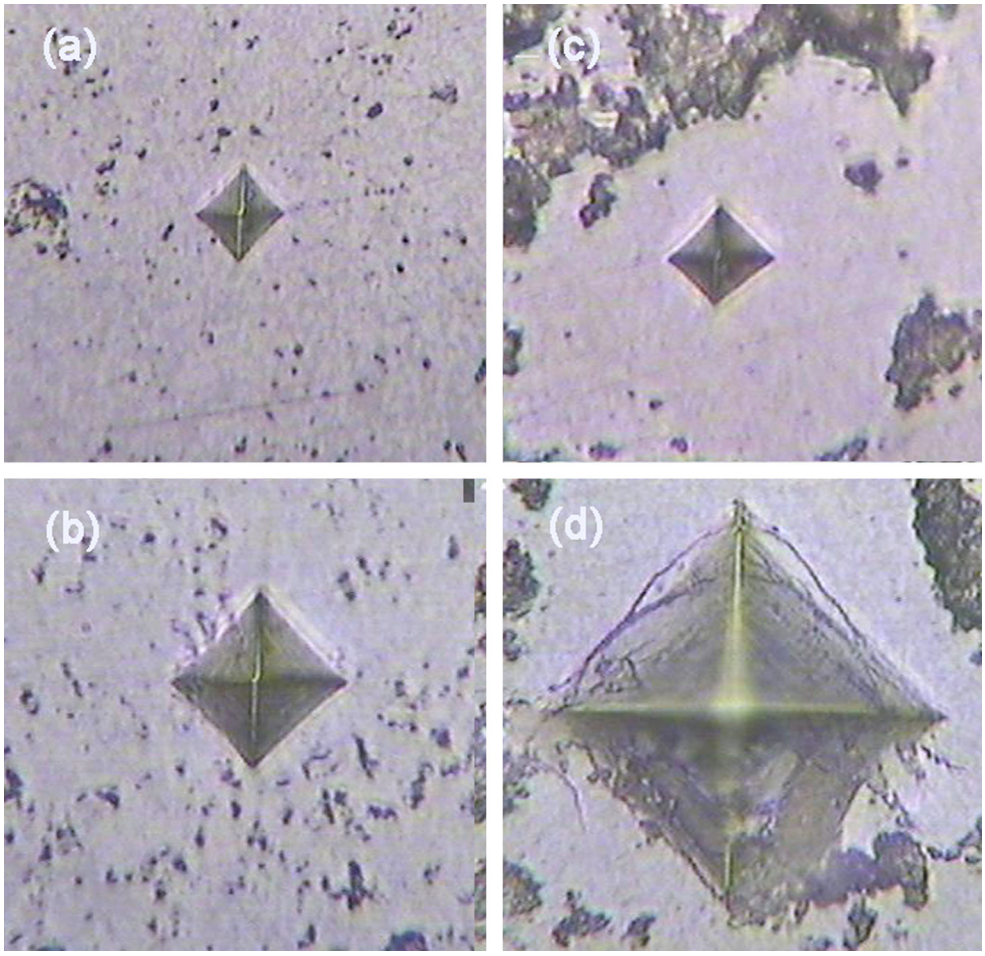

Fig. 10. Indentation impressions on the sample surface: (a) sample NY00, $P=0.49$ N; (b) sample NY00, $P=1.96$ N; (c) sample NY20, $P=0.49$ N; (C) sample NY20, $P=1.96$ N.

load range. If one writes out all the energy terms to establish a reasonable energy-balance relation similar to Eqs. (6) or (10), however, a true hardness number, H_T, may be obtained by analyzing the variation of a_2 with some certain microstructural parameters. In continuation of this idea, it is suggested here that, when using the modified PSR model, Eq. (4), to describe the indentation data measured on a given material system, it should be ensured carefully that the energy changes during indentation are dominated by the same mechanisms within the whole test load range.

5. Conclusions

A series of NiO–ZrO_2 composite ceramics with different porosities were prepared and the microhardness were measured using a Vickers indenter in the load range of 0.49–4.9 N. By analyzing the experimental measured indentation data, the following conclusions were obtained:

(1) Indentation size effect, i.e., the decreasing tendency in the measured hardness with increasing applied test load, is observed in all the examined samples and the modified proportional specimen resistance (PSR) model is proven to be suitable for describing the indentation data in each case.
(2) The load-independent hardness, which is calculated based on the modified PSR model, exhibits a significant dependence on the porosity of the test material. This porosity dependence may be explained reasonably based on the simple and phenomenological model proposed by Gong [31].
(3) Further analyzing the effect of porosity on the microhardness tests suggests that, when using the modified PSR model, Eq. (4), to describe the indentation data measured on a given material system, it should be ensured carefully that the energy changes during indentation are dominated by the same mechanisms within the whole test load range.

References

[1] D. Chakraborty, J. Mukerji, Characterization of silicon nitride single crystals and polycrystalline reaction sintered silicon nitride by microhardness measurements, Journal of Materials Science 15 (1980) 3051–3056.
[2] K. Hirao, M. Tomozawa, Microhardness of SiO_2 glass in various environments, Journal of the American Ceramic Society 70 (1987) 497–502.
[3] G.N. Babini, A. Bellosi, C. Galassi, Characterization of hot-pressed silicon nitride based materials by microhardness measurements, Journal of Materials Science 22 (1987) 1687–1693.
[4] A.K. Mokhopadhyay, S.K. Datta, D. Chakraborty, On the microhardness of silicon nitride and sialon ceramics, Journal of the European Ceramic Society 6 (1990) 303–311.
[5] J.B. Quinn, G.D. Quinn, Indentation brittleness of ceramics: a fresh approach, Journal of Materials Science 32 (1997) 4331–4346.
[6] H. Kim, T. Kim, Measurement of hardness on traditional ceramics, Journal of the European Ceramic Society 22 (2002) 1437–1445.
[7] Z.H. Xie, M. Hoffman, Y.B. Cheng, Microstructural tailoring and characterization of a calcium α-SiAlON composition, Journal of the American Ceramic Society 85 (2002) 812–818.
[8] L. Sidjanin, D. Rajnovic, J. Ranogajec, E. Molnar, Measurement of Vickers hardness on ceramic floor tiles, Journal of the European Ceramic Society 27 (2007) 1767–1773.
[9] J. Zou, G.J. Zhang, Y.M. Kan, P.L. Wang, Hot-pressed ZrB_2-SiC ceramics with VC addition: chemical reactions, microstructures, and mechanical properties, Journal of the American Ceramic Society 92 (2009) 2838–2846.
[10] C. Terzioglu, Instigation of some physical properties of Gd added Bi-2233 superconductors, Journal of Alloys and Compounds 509 (2011) 87–93.
[11] F. Fröhlich., P. Grau, W. Grellmann, Performance and analysis of recording microhardness tests. Phys, Status Solidi 42 (1977) 79–89.
[12] H. Li, R.C. Bradt, The microhardness indentation load/size effect in rutile and cassiterite single crystals, Journal of Materials Science 28 (1993) 917–926.
[13] J.H. Gong, J.J. Wu, Z.D. Guan, Examination of the indentation size effect in low-load Vickers hardness testing of ceramics, Journal of the European Ceramic Society 19 (1999) 2625–2631.
[14] J.H. Gong, Y. Li, An energy-balance analysis for the size effect in low-load hardness testing, Journal of Materials Science 35 (2000) 209–213.
[15] K. Sangwal, Review: indentation size effect, indentation cracks and microhardness measurement of brittle crystalline solids – some basic concepts and trends, Crystal Research and Technology 44 (2009) 1019–1037.
[16] D.Y. Jiang, Recent progresses in the phenomenological description for the indentation size effect in microhardness testing of brittle ceramics, Journal of Advanced Ceramics 1 (2012) 38–49.
[17] H. Bückle, Mikrohärteprüfung. Berliner Union Verlag, Stuttgart, Germany, 1965.
[18] B.D. Michels, G.H. Frischa, Microhardness of chalcogenide glasses of the system Se-Ge-As, Journal of Materials Science 17 (1982) 329–334.
[19] J.H. Gong, J.J. Wu, Z.D. Guan, Load dependence of the apparent hardness of silicon nitride ceramics in a wide range of loads, Materials Letters 35 (1998) 58–61.
[20] J.H. Gong, Z. Zhao, Z.D. Guan, H.Z. Miao, Load-dependence of Knoop hardness of Al_2O_3-TiC composites, Journal of the European Ceramic Society 20 (2000) 1895–1900.
[21] J.H. Gong, J.J. Wu, Z.D. Guan, Load dependence of low-load Knoop hardness in ceramics: a modified PSR model, Materials Letters 47 (2001) 140–144.
[22] J.H. Gong, H.Z. Miao, Z. Zhao, Z.D. Guan, Load-dependence of the measured hardness of Ti(C,N)-based cermets, Materials Science and Engineering A303 (2001) 179–186.
[23] K. Sangwal, B. Surowska, P. Blaziak, Analysis of the indentation size effect in the microhardness measurement of some cobalt-based alloys, Materials Chemistry and Physics 77 (2002) 511–520.
[24] E. Atar, H. Cimenoglu, E.S. Kayali, Hardness characterization of thin Zr (Hf,N) coatings, Surface and Coatings Technology 162 (2003) 167–173.
[25] U. Kölemen, Analysis of ISE in microhardness measurements of bulk MgB_2 superconductors using different models, Journal of Alloys and Compounds 425 (2006) 429–435.
[26] O. Sahin, O. Uzun, M. Sopicka-Lizer, H. Gocmez, U. Kölemen, Dynamic hardness and elastic modulus calculation of porous SiAlON ceramics using depth-sensing indentation technique, Journal of the European Ceramic Society 28 (2008) 1235–1242.
[27] C.T. Rios, A.A. Coelho, W.W. Batista, M.C. Goncalves, R. Caram, ISE and fracture toughness evaluation by Vickers hardness testing of an Al_3Nb-Nb_2Al-AlNbNi in situ composite, Journal of Alloys and Compounds 472 (2009) 65–70.
[28] T. Filetin, S. Solic, I. Zmak, The indentation size effect on the microhardness of sea mollusk shell structures, Materials Testing 53 (2011) 48–53.
[29] M.A. Camerucci, G. Urretavizcaya, A.L. Cavalieri, Mechanical behavior of cordierite and cordierite-mullite materials evaluated by indentation techniques, Journal of the European Ceramic Society 21 (2001) 1195–1204.
[30] S. Roy, B.S.S. Chandra Rao, J. Subrahmanyam, Evaluation of mechanical properties of gelcast lead zirconate titanate disks sintered at different temperatures, Scripta Materialia 57 (2007) 1024–1027.

[31] J.H. Gong, Comment on Measurement of hardness on traditional ceramics, Journal of the European Ceramic Society 23 (2003) 1769–1772.

[32] A. Tricoteaux, E. Rguiti, D. Chicot, L. Boilet, M. Descamps, A. Leriche, J. Lesage, Influence of porosity on the mechanical properties of microporous β-TCP bioceramics by usual and instrumented Vickers microindentation, Journal of the European Ceramic Society 31 (2011) 1261–1369.

[33] W.D. Nix, H. Gao, Indentation size effects in crystalline materials: a law for strain gradient plasticity, Journal of the Mechanics and Physics of Solids 46 (1998) 411–425.